Journal of the European Ceramic Society 43 (2023) 2039–2044

Contents lists available at ScienceDirect

Journal of the European Ceramic Society

journal homepage: www.elsevier.com/locate/jeurceramsoc

Measurement of ceramics cracking during water quenching by digital image correlation

Yuqiao Li [a,c,1], Qingxian Li [a,c,1], Chuandong Zuo [a,c], Fei Qi [b], Long Li [a,c], Jiachen Wei [a,c], Yingfeng Shao [a,c,*], Fan Song [a,c,*]

[a] State Key Laboratory of Nonlinear Mechanics and Beijing Key Laboratory of Engineered Construction and Mechanobiology, Institute of Mechanics, Chinese Academy of Sciences, Beijing 100190, China
[b] School of Mechanical and Electric Engineering, Soochow University, Suzhou 215021, China
[c] School of Engineering Science, University of Chinese Academy of Sciences, Beijing 100049, China

ARTICLE INFO

Keywords:
Thermal shock
Digital image correlation
Ceramics
Crack propagation
Crack speed

ABSTRACT

Measuring the thermal shock crack growth process is crucial for revealing ceramic materials and structures' thermal shock failure mechanisms and evaluating their reliability. We used a self-made water quenching system to conduct thermal shock tests on alumina and zirconia ceramics. The thermal shock process was recorded by high-speed digital image correlation (DIC) during the test. The process of thermal shock crack initiation and propagation in two kinds of ceramics was determined by analyzing the speckle image change on the sample's surface. It is found that the crack growth rate of alumina is faster than that of zirconia, which is caused by different material parameters. This paper presents an in-situ measurement method for the initiation and propagation of thermal shock cracking in ceramic materials. It can provide a measurement method to identify and predict the thermal shock damage of ceramic components.

1. Introduction

Due to the brittleness of ceramics, it is easy to cause thermal shock failure due to uneven deformation when the ambient temperature changes sharply, an inherent defect of ceramic materials [1]. Generally, the thermal shock performance of ceramic is evaluated using water quenching [2–4], flame [5], irradiation [6], and laser [7]. The critical parameters in the evaluation are the crack morphology and residual strength of specimens after thermal shock [6–11]. However, these experimental results are all after thermal shock, and there is little experimental verification of real-time crack growth. The real-time results are very important for studying damage mechanisms [8]. We observed and studied the real-time thermal shock crack propagation of translucent alumina ceramics in the early stage [8,9]. The reflection and refraction of light can record the crack propagation under thermal shock. But for the vast majority of non-transparent ceramics, it seems powerless.

In the recent ten years, there have been a lot of theoretical studies on the initiation and propagation of thermal shock cracks [10–15]. Remarkable scientific progress has been achieved in the initiation and propagation of thermal shock cracks in ceramics, but mainly for alumina ceramics. Therefore, it is urgent to develop a method that can measure the thermal shock cracking of opaque ceramics in real time to evaluate the failure process of ceramic thermal shock and understand the failure mechanism.

Digital image correlation (DIC) has been widely used to measure the deformation field evolution of solid materials in many fields [16–20]. It also includes the crack characterization of brittle materials after thermal shock cycles [19,20]. The above is the characterization under the uniform field temperature field. However, there are few reports on thermal shock crack identification under the time-varying temperature field. It may be challenging to solve such problems because it needs to fully and accurately understand materials' mechanical and physical properties as well as the actual initial and boundary conditions.

This study aims to develop an experimental method for the real-time measurement of thermal shock cracks. Using the designed real-time observation device of water quenching and DIC, we have observed and studied the initiation and propagation of thermal shock cracks in

* Corresponding authors at: State Key Laboratory of Nonlinear Mechanics and Beijing Key Laboratory of Engineered Construction and Mechanobiology, Institute of Mechanics, Chinese Academy of Sciences, Beijing 100190, China
E-mail addresses: shaoyf@lnm.imech.ac.cn (Y. Shao), songf@lnm.imech.ac.cn (F. Song).
[1] These authors equally contributed to this work.

https://doi.org/10.1016/j.jeurceramsoc.2022.12.060
Received 22 September 2022; Received in revised form 7 December 2022; Accepted 23 December 2022
Available online 24 December 2022
0955-2219/© 2022 Elsevier Ltd. All rights reserved.

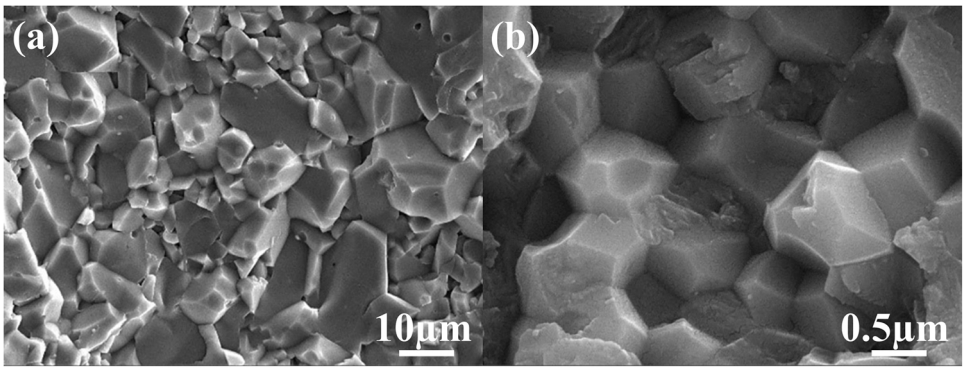

Fig. 1. SEM of fracture surface of ceramics (a) Al_2O_3, (b) 3Y-ZrO_2.

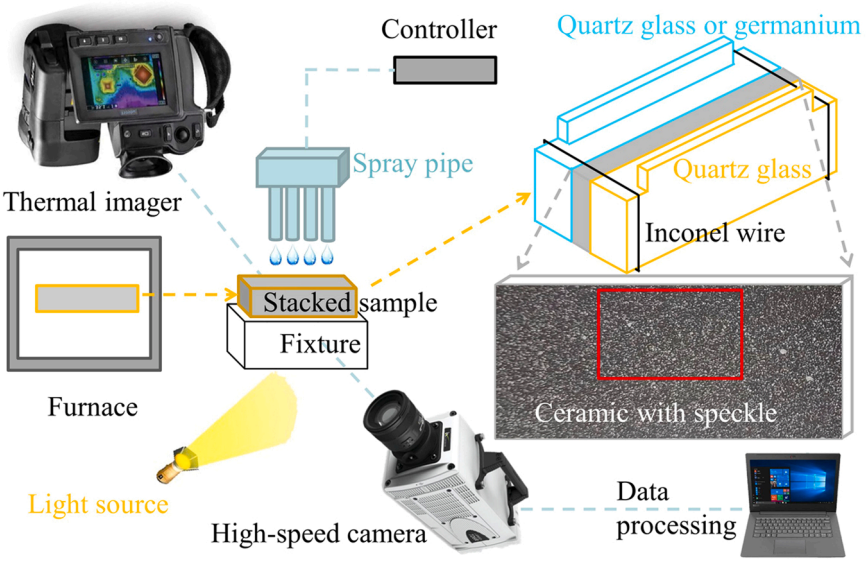

Fig. 2. Schematic illustration of the experimental setup of the water quenching thermal shock and digital image correlation.

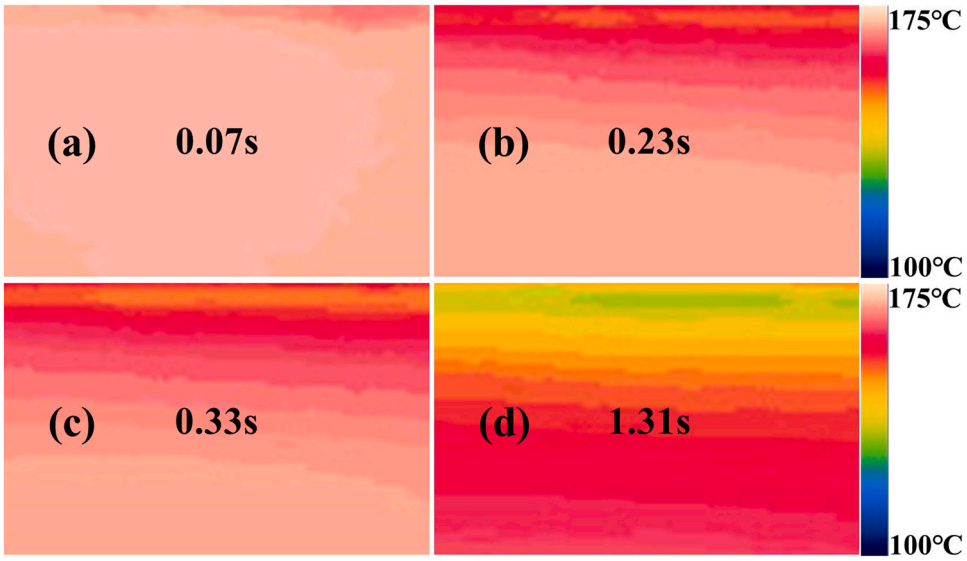

Fig. 3. The corresponding temperature field change of the test area during the thermal shock of Al_2O_3 at 160 °C (a) 0.07 s, (b) 0.23 s, (c) 0.33 s, (d) 1.31 s.

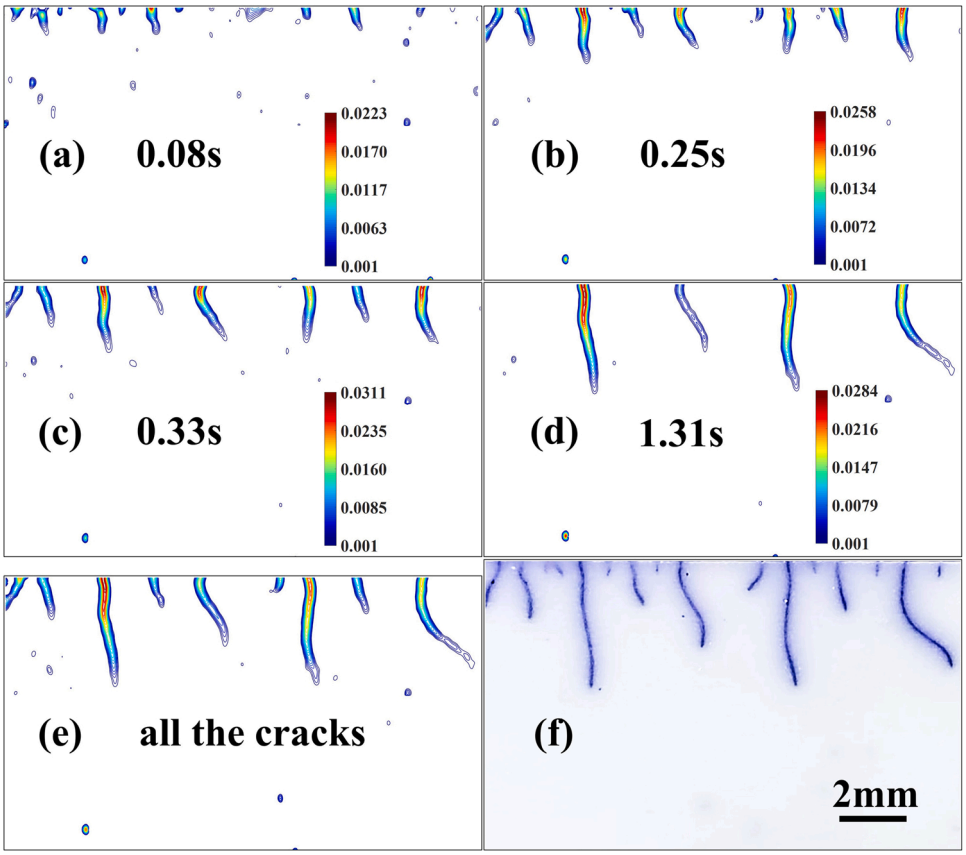

Fig. 4. (a) - (d) the DIC horizontal strain field change with time during the thermal shock of Al_2O_3, (e) all the cracks that appear and disappear in the above process, and (f) the cracks taken from dyeing after thermal shock.

two opaque ceramic materials, Al_2O_3 and 3Y-ZrO_2. They are selected because they significantly differ in thermal conductivity and fracture toughness, and our previous simulation finds that they have a significant difference in crack growth rate [21]. So, the difference in crack growth rate between the two ceramics is also compared.

2. Experiment

2.1. Materials and preparation

We purchased the Al_2O_3 (grain size 7.5 μm) and 3Y-ZrO_2 (grain size 0.6 μm) from Zhuhai Jiawei Ceramics Co., Ltd., China. The above ceramics have the size of 1 mm × 10 mm × 50 mm and are prepared by tape casting method. The fracture surfaces of the ceramics are shown in Fig. 1.

2.2. Speckle preparation

We made unified speckle preparation for the two specimens. That is, spray a thin layer of black speckle on the surface of 50 × 10 mm^2, then spray white speckle randomly to use a CCD camera to record the instantaneous change of the specimen's surface and obtain the image of the strain field, as shown in Fig. 2. The speckle thickness is controlled below 0.025 mm compared with the 1 mm thick sample to reduce the influence on the deformation of the sample.

We use high-temperature speckles (Gootgt-201, Shenzhen Gangtu Trading Co., Ltd., China), which can be used at 600 °C. It meets the speckle requirements of our test temperature of 400 °C. We adopted the speckle pattern assessment software (Glare) and measured that the speckle size was between 4.68 and 4.94 pixels [22]. We also found that the average gray gradient was between 21.59 and 23.27 [22]. The above key parameters meet the requirements of standard speckle calculation [22,23].

2.3. Thermal shock test

The thermal shock test of the sample is carried out by water quenching. We use two quartz glass fixtures to clamp the speckled ceramic sheet into a sandwich structure, as shown in Fig. 2. Put the sample into the muffle furnace with the temperature of 400 °C, keep it for 30 min, and then quickly take it out (within 5 s) and place it on a fixture with a pre-focused position. Tubes above the sample start to spray water downward for 0.3 s at the speed of 4 ml/s for the test. Meanwhile, the high-speed camera (phantom V2020, Wayne, NJ, USA) facing the sample collects speckle images during thermal shock at 1000 frames / s. We selected a rectangular area of 14.62 × 9.69 mm^2 (1280 × 800 pixels) from the speckle images of the specimen for calculation, as shown in Fig. 2.

We use a germanium window instead of a quartz glass to observe the temperature change of ceramic during water quenching with a thermal imager (FLIR T650sc FLIR Systems, Wilsonville, OR, USA). The corresponding temperature measurement results of the test area are shown in Fig. 3 and supplementary video S1. Because the germanium window cannot withstand high-temperature water quenching, we measured the temperature change of the test at 160 °C instead. As expected, the temperature change during water quenching is relatively uniform along the horizontal direction.

2.4. Measurement of surface strain fields

The DIC method is a technology to measure the changes in images of an object before and after surface deformation. Based on the DIC

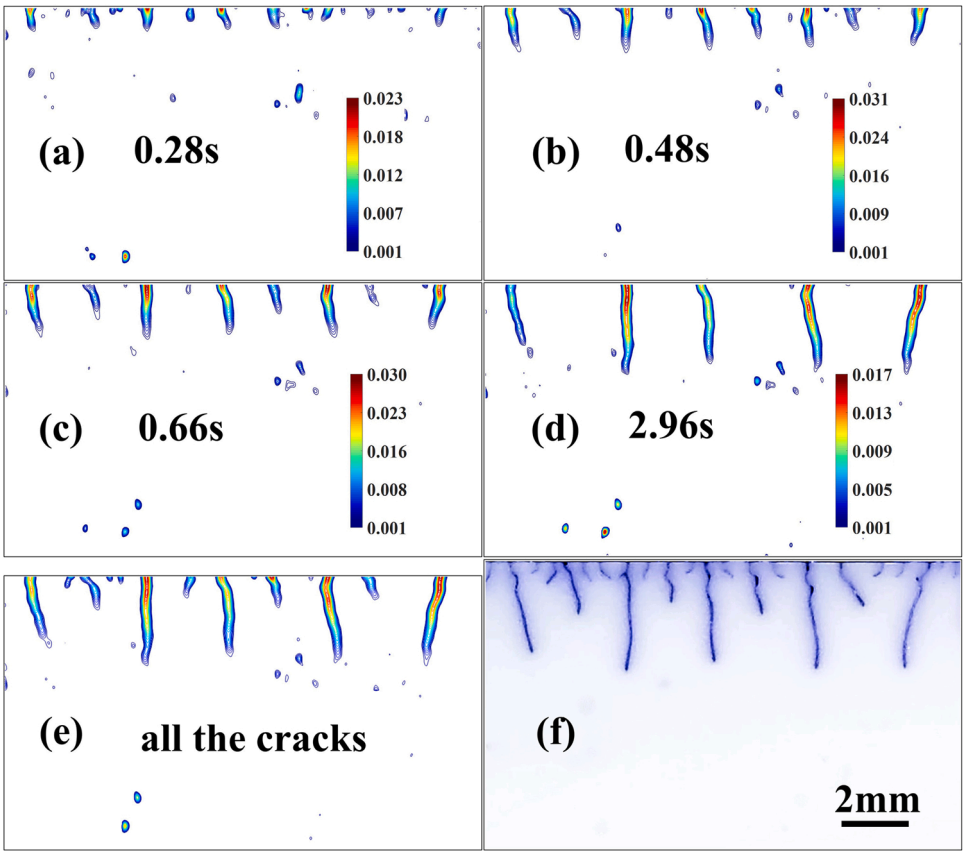

Fig. 5. (a) - (d) the DIC horizontal strain field change with time during the thermal shock of 3Y-ZrO_2, (e) all the cracks that appear and disappear in the above process, and (f) the cracks taken from dyeing after thermal shock.

Table 1
Crack growth rates of Al_2O_3 and 3Y-ZrO_2 calculated by DIC under thermal shock.

Average speed (mm/s)	Al_2O_3	3Y-ZrO_2
0.2 s	5.96 ± 0.92	2.32 ± 0.42
Whole process	2.40 ± 0.58	0.91 ± 0.06

method, the changes of horizontal and vertical strains on the ceramic surface can be obtained during the fracture process under thermal shock. Because the thermal shock surface is horizontal, the quartz window has a temperature gradient in the vertical direction during quenching. The refractive index in the vertical direction will be different, and a stress gradient will also be introduced. Therefore, the speckles of the test will introduce errors in the measurement of vertical strain when they pass through the quartz glass to the camera [24]. The temperature can be considered relatively uniform in the horizontal direction, as seen in Fig. 3 and supplementary video S1. In this way, because the refraction of light is basically the same, the error introduced in the measurement of horizontal strain will be tiny. In addition, because the crack mainly propagates along the vertical direction, we use the horizontal strain as the basis for identifying the crack.

Usually, we need to use mechanical strain as the comparison of strain field, that is, by subtracting temperature strain from DIC measured strain. Because of the temperature uniformity in the horizontal direction, the total DIC measured strain is used here to replace the mechanical

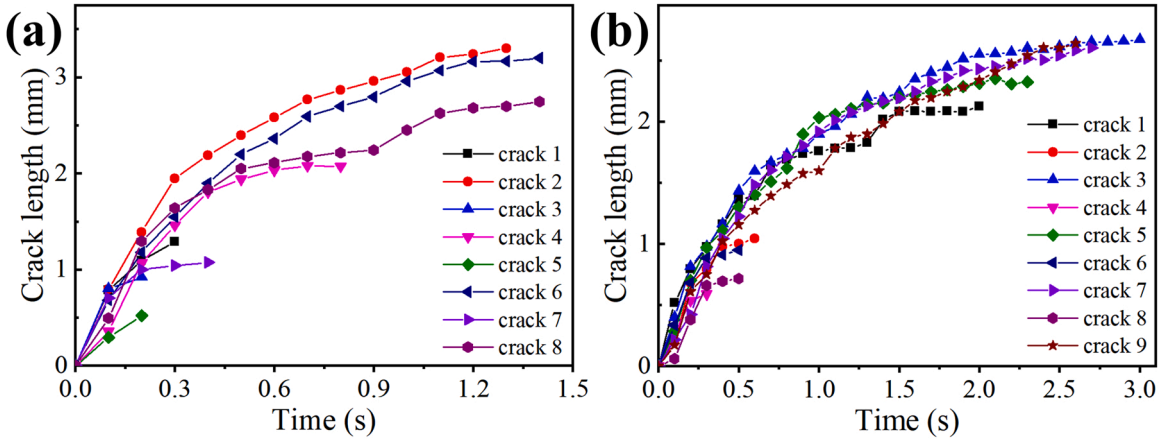

Fig. 6. Crack lengths change with time calculated by DIC under thermal shock (a) Al_2O_3, and (b) 3Y-ZrO_2.

strain. By this method, we successfully observed the propagation of the thermal shock cracks. We can obtain the average crack growth rate through different crack lengths from a series of images recorded in the experiment.

We use the open-source DIC program, Ncorr, to analyze the collected images [25]. During calculation, the subset size of 21 pixels and step size of 2 pixels were selected to calculate the displacement field, and then the strain filter size of 11 was selected to calculate the strain field.

2.5. Crack comparison

Because the ceramics are opaque, we dye the cracks of the ceramics after thermal shock. Put the water-quenched sample in blue ink (Shanghai ink factory, Shanghai, China) for 1 min, then take it out and dry it. The crack morphology on the back of the speckled surface can be obtained by scanning with a scanner and comparing them with the DIC results.

3. Result and discussion

Fig. 4 and supplementary video S2 show the DIC horizontal strain field change with time during the thermal shock of Al_2O_3 and the cracks taken from dyeing after thermal shock.

For Al_2O_3, the DIC strain field obtained from the thermal shock test sample shows a non-uniform horizontal strain ε_x distribution when water contacts the sample for about 0.08 s, as shown in Fig. 4a. Several areas appear at certain intervals near the upper surface in contact with water, among which the extreme values of ε_x exceed the threshold value of 0.001, indicating that the sample shrinks under the influence of water quenching and small cracks that start and go forward appear. At about 0.25 s, some short cracks stop growing, and the remaining long cracks continue to grow. That is, crack hierarchy occurs [9,14], as shown in Fig. 4b. At about 0.33 s, the short crack that did not grow slowly shrinks back, and the long crack continues to grow, as shown in Fig. 4c. It is because the tensile stress is large when the small cracks grow together before. Still, when the long crack grows, the tensile stress in the small crack area gradually decreases. Hence, the virtual strain gradually decreases and cannot be identified (of course, the temperature strain also has a certain influence). At about 1.31 s, the small cracks have disappeared, and the long cracks have reached the maximum, as shown in Fig. 4c. Similarly, at about 2.31 s, the long crack also became shorter. Fig. 4e is a DIC crack diagram that draws all the cracks that appear and disappear in the above process. We can see that it is in good agreement with the results of the dyeing test, as shown in Fig. 4f. Note that there is about 0.3 mm speckle contact with water during the test, which will introduce some errors in the speckle calculation. Therefore, we did not use the data about 0.45 mm from the surface, which is the length of most short cracks. The above phenomena also show that measuring crack growth under thermal shock is challenging. In addition, the thermal shock crack growth of alumina identified by DIC technology during water quenching is consistent with that of translucent alumina in the previous study [9].

Fig. 5 and supplementary video S3 show the DIC horizontal strain field change with time during the thermal shock of 3Y-ZrO_2 and the cracks taken from dyeing after thermal shock. We can see that 3Y-ZrO_2 has a crack hierarchy structure similar to Al_2O_3. The DIC strains' crack growth and disappearance phenomenon are also very close. Similarly, when all cracks are in the most extended state, we can see that the DIC cracks are in good agreement with the results after the dyeing test, as shown in Fig. 5e and f.

We can get the full-field crack map at different thermal shock times through the DIC method. Through comparison, it is found that the effect of full-field crack identification is excellent, which can directly reflect the crack propagation on the surface of ceramic materials.

However, we find that the crack growth rates of Al_2O_3 and 3Y-ZrO_2 are different. We selected the longest four cracks for comparison. We can see that the crack growth rate of alumina is close to three times that of zirconia, as shown in Table 1 and Fig. 6. It is mainly because alumina has a lower fracture toughness and a higher thermal conductivity than zirconia, which is consistent with our previous calculation of phase-field [21].

4. Conclusions

Water quenching thermal shock experiments were carried out on opaque Al_2O_3 and 3Y-ZrO_2 ceramic materials. We used DIC technology to measure the thermal shock cracks in situ. The results show that the crack morphologies of the two ceramics after water quenching by DIC technology are very close to the dyeing method. The thermal shock crack growth of Al_2O_3 identified by DIC technology during water quenching is consistent with that of translucent Al_2O_3 in the early stage. It can be considered that this paper presents an in-situ measurement method for the initiation and propagation of water-quenched thermal shock cracks in opaque ceramics. In addition, it is also found that alumina's thermal shock crack growth rate is faster than that of zirconia due to different material properties.

Declaration of Competing Interest

The authors declare that they have no known competing financial interests or personal relationships that could have appeared to influence the work reported in this paper.

Acknowledgments

This work was sponsored by the National Natural Science Foundations of China [Grant Nos. 12232019, 11972041]; Youth Innovation Promotion Association CAS; the Science Foundation of the National Key Laboratory of Science and Technology on Advanced Composites in Special Environments [Grant No. JCKYS2020603C017].

References

[1] J.C. Han, B.L. Wang, Thermal shock resistance of ceramics with temperature-dependent material properties at elevated temperature, Acta Mater. 59 (2011) 1373–1382, https://doi.org/10.1016/j.actamat.2010.10.068.
[2] H.A. Bahr, G. Fischer, H.J. Weiss, Thermal-shock crack patterns explained by single and multiple crack-propagation, J. Mater. Sci. 21 (1986) 2716–2720, https://doi.org/10.1007/BF00551478.
[3] T. Yoshimoto, S. Ishihara, T. Goshima, A.J. McEvily, T. Ishizaki, An improved method for the determination of the maximum thermal stress induced during a quench test, Scr. Mater. 41 (1999) 553–559, https://doi.org/10.1016/S1359-6462(99)00185-2.
[4] D.Y. Li, W.G. Li, W.B. Zhang, D.N. Fang, Thermal shock resistance of ultra-high temperature ceramics including the effects of thermal environment and external constraints, Mater. Des. 37 (2012) 211–214, https://doi.org/10.1016/j.matdes.2011.12.047.
[5] S.R. Levine, E.J. Opila, M.C. Halbig, J.D. Kiser, M. Singh, J.A. Salem, Evaluation of ultra-high temperature ceramics for aeropropulsion use, J. Eur. Ceram. Soc. 22 (2002) 2757–2767, https://doi.org/10.1016/S0955-2219(02)00140-1.
[6] G.A. Schneider, G. Petzow, Thermal shock testing of ceramics-a new testing method, J. Am. Ceram. Soc. 74 (1991) 98–102, https://doi.org/10.1111/j.1151-2916.1991.tb07303.x.
[7] C.Y. Jian, T. Hashida, H. Takahashi, M. Saito, Thermal shock and fatigue resistance evaluation of functionally graded coating for gas turbine blades by laser heating method, Compos. Eng. 5 (1995) 879–889, https://doi.org/10.1016/0961-9526(95)00041-K.
[8] Q.X. Li, Y.Q. Li, J. Li, L. Li, X.F. Wu, Y.F. Shao, Y. Charles, S. Barboura, F. Song, Prefabricated crack propagation in translucent alumina ceramic sheets during flame thermal shock, Eng. Fract. Mech. 263 (2022), 108285, https://doi.org/10.1016/j.engfracmech.2022.108285.
[9] Y.F. Shao, B.Y. Liu, X.H. Wang, L. Li, J.C. Wei, F. Song, Crack propagation speed in ceramic during quenching, J. Eur. Ceram. Soc. 38 (7) (2018) 2879–2885, https://doi.org/10.1016/j.jeurceramsoc.2018.02.028.
[10] T. Wang, X. Ye, Z.L. Liu, X.M. Liu, D.Y. Chu, Z. Zhuang, A phase-field model of thermo-elastic coupled brittle fracture with explicit time integration, Comput. Mech. 65 (2020) 1305–1321, https://doi.org/10.1007/s00466-020-01820-6.
[11] D.Y. Li, P.D. Li, W.D. Li, W.G. Li, K. Zhou, Three-dimensional phase-field modeling of temperature-dependent thermal shock-induced fracture in ceramic materials, Eng. Fract. Mech. 268 (2022), 108444, https://doi.org/10.1016/j.engfracmech.2022.108444.

[12] S.B. Tang, H. Zhang, C.A. Tang, H.Y. Liu, Numerical model for the cracking behavior of heterogeneous brittle solids subjected to thermal shock, Int. J. Solid Struct. 80 (2016) 520–531, https://doi.org/10.1016/j.ijsolstr.2015.10.012.
[13] J. Li, F. Song, C.P. Jiang, Direct numerical simulations on crack formation in ceramic materials under thermal shock by using a non-local fracture model, J. Eur. Ceram. Soc. 33 (2013) 2677–2687, https://doi.org/10.1016/j.jeurceramsoc.2013.04.012.
[14] Y.T. Wang, X.P. Zhou, M.M. Kou, An improved coupled thermo-mechanic bondbased peridynamic model for cracking behaviors in brittle solids subjected to thermal shocks, Eur. J. Mech. Solid. 73 (2019) 282–305, https://doi.org/10.1016/j.euromechsol.2018.09.007.
[15] B. Bourdin, J.J. Marigo, C. Maurini, P. Sicsic, Morphogenesis and propagation of complex cracks induced by thermal shocks, Phys. Rev. Lett. 112 (2014), 014301, https://doi.org/10.1103/PhysRevLett.112.014301.
[16] L.N. Gu, W.R. Gong, X.X. Shao, J. Chen, Z.Q. Dong, G. Wu, X.Y. He, Real time measurement and analysis of full surface cracking characteristics of concrete based on principal strain field, Chin. J. Theor. Appl. Mech. 53 (7) (2021) 1962–1970.
[17] F. Yuan, L. Cheng, X.X. Shao, Z.Q. Dong, L. Zhang, G. Wu, X.Y. He, Full-field measurement and fracture and fatigue characterizations of asphalt concrete based on the SCB test and stereo-DIC, Eng. Fract. Mech. 235 (2020), 107127, https://doi.org/10.1016/j.engfracmech.2020.107127.
[18] Y. Dai, D. Gruber, H. Harmuth, Observation and quantification of the fracture process zone for two magnesia refractories with different brittleness, J. Eur. Ceram. Soc. 37 (6) (2017) 2521–2529, https://doi.org/10.1016/j.jeurceramsoc.2017.02.005.
[19] P.Y. Yu, P.Z. Pan, G.L. Feng, Z.H. Wu, S.K. Zhao, Physico-mechanical properties of granite after cyclic thermal shock, J. Rock Mech. Geotech. 12 (2020) 693–706, https://doi.org/10.1016/j.jrmge.2020.03.001.
[20] C. Bumgardner, B. Croom, X.D. Li, High-temperature delamination mechanisms of thermal barrier coatings: in-situ digital image correlation and finite element analyses, Acta Mater. 128 (2017) 54–63, https://doi.org/10.1016/j.actamat.2017.01.061.
[21] C.D. Zuo, Q.X. Li, Q. Wang, Y.Q. Li, L. Li, J.C. Wei, Y.F. Shao, F. Song, Effect of material parameters on thermal shock crack of ceramics calculated by phase-field method, J. Am. Ceram. Soc. (2022), https://doi.org/10.1111/jace.18720.
[22] Y. Su, Q. Zhang, Glare: A free and open-source software for generation and assessment of digital speckle pattern, Opt. Laser Eng. 148 (2022), 106766, https://doi.org/10.1016/j.optlaseng.2021.106766.
[23] B. Pan, Z. Lu, H. Xie, Mean intensity gradient: an effective global parameter for quality assessment of the speckle patterns used in digital image correlation, Opt. Laser Eng. 48 (4) (2010) 469–477, https://doi.org/10.1016/j.optlaseng.2009.08.010.
[24] C. Periasamy, H.V. Tippur, Measurement of orthogonal stress gradients due to impact load on a transparent sheet using digital gradient sensing method, Exp. Mech. 53 (2013) 97–111, https://doi.org/10.1007/s11340-012-9653-x.
[25] J. Blaber, B. Adair, A. Antoniou, Ncorr: open-source 2D digital image correlation matlab software, Exp. Mech. 55 (6) (2015) 1105–1122, https://doi.org/10.1007/s11340-015-0009-1.